



## Research Article

# Peroxymonosulfate Activation on a Hybrid Material of Conjugated PVC and TiO<sub>2</sub> Nanotubes for Enhancing Degradation of Rhodamine B under Visible Light

La Phan Phuong Ha,<sup>1,2</sup> Tran Hong Huy,<sup>1,2</sup> Pham Huu Huan,<sup>1,2</sup> Nguyen Thi Minh Thu,<sup>1,2</sup> Cao Minh Thi <sup>3</sup> and Pham Van Viet <sup>1,2</sup>

<sup>1</sup>Faculty of Materials Science and Technology, University of Science, VNU-HCM, 227 Nguyen Van Cu Street, District 5, Ho Chi Minh City 700000, Vietnam

<sup>2</sup>Vietnam National University-Ho Chi Minh City, Linh Trung Ward, Thu Duc District, Ho Chi Minh City 700000, Vietnam

<sup>3</sup>Ho Chi Minh City University of Technology (HUTECH), 475A Dien Bien Phu Street, Binh Thanh District, Ho Chi Minh City 700000, Vietnam

Correspondence should be addressed to Cao Minh Thi; [cmthi@hutech.edu.vn](mailto:cmthi@hutech.edu.vn) and Pham Van Viet; [pvviet@hcmus.edu.vn](mailto:pvviet@hcmus.edu.vn)

Received 29 August 2020; Revised 28 October 2020; Accepted 30 October 2020; Published 26 November 2020

Academic Editor: Hoang Vinh Tran

Copyright © 2020 La Phan Phuong Ha et al. This is an open access article distributed under the Creative Commons Attribution License, which permits unrestricted use, distribution, and reproduction in any medium, provided the original work is properly cited.

Visible-light-driven photocatalysis is a robust technology for amending the negative effect of pollutants on the environment with a minimum energy use. Herein, we describe a simple approach to producing such a photocatalyst by coupling conjugated polyvinyl chloride (cPVC) with the TiO<sub>2</sub> nanotube (TNT) thermolysis method. By activating peroxymonosulfate (PMS) to make a cPVC/TNT/PMS system using visible light as the source, we obtain a significant enhancement in the photocatalytic performance. We show that PMS use at a concentration of 3 mM can fully degrade rhodamine B (RhB) solution at a remarkably high concentration (200 mg L<sup>-1</sup>) just in 120 min under visible light. The cPVC/TNT/PMS system also shows excellent stability in recycling tests for at least five times. Further, by confining the active species in photocatalytic reactions, we report a thorough understanding of the extent of involvement from those radicals. Our work presents a robust approach to make a high-performance, visible-light-driven photocatalyst, which can be potentially used in practice.

## 1. Introduction

Photocatalysis technology is a great means of treating environmental pollutants by making direct use of light to generate highly active oxygen species that are more favorable because of the high performance, environmental benefits, and low operating cost [1–4]. For photocatalytic materials to be used widely in practice, the source of the exciting light should be abundantly available (i.e., visible light that accounts for about 43% of the solar radiation and does not require any energy to be produced); the preparation of photocatalysts should also be simple, inexpensive, and robust [5, 6].

Recently, sulfate radical anion- (SO<sub>4</sub><sup>-</sup>) induced advanced oxidation reactions that have been successfully used in treating organic pollutants in water [7–9]. In comparison with hydroxyl radical (·OH), SO<sub>4</sub><sup>-</sup> has a higher reduction potential [10]. Also, SO<sub>4</sub><sup>-</sup> has advantages such as pH independence [11], greater oxidation selectivity of organic pollutants, and longer lifetime during the reaction [12]. Peroxymonosulfate (PMS) activation-induced SO<sub>4</sub><sup>-</sup> is usually generated via thermolysis, photolysis, photocatalysis, a metallic oxidant, and carbon materials [13–16]. Therein, activation of PMS assisted by a photocatalyst under visible light is environmentally sustainable and simple to perform without additional energy/chemical requirement.

Previous studies have shown that the combination of photocatalytic materials with readily available polymers after being conjugated would lead to the production of barely expensive nanocomposites but having a promising photocatalytic performance [17–23]. For instance, a conjugated polyvinyl chloride- (cPVC-) grafted  $\text{SnS}_2$  nanocomposite, having a high photocatalytic performance in the reduction of aqueous Cr(VI) under visible light, was reported [18]. More recently, getting combined PANI and  $\text{Ag}_3\text{PO}_4$ , a highly efficient visible-light-driven photocatalyst with a core@shell structure was prepared [20]. Although visible-light-driven photocatalysts have been extensively reported for years, complex steps in preparation and low efficiency remain a major challenge for such photocatalysts to be used broadly and effectively [24–28]. Noticeably, a recent study has reported a prominently facile approach to produce a nanocomposite of conjugated polyvinyl chloride (cPVC) and  $\text{TiO}_2$  nanotubes (TNTs), showing a remarkable photocatalytic performance under visible light [29]. By taking advantage of the ability for mass production of TNT with the abundant availability, chemical stability, and ease in the processing of cPVC, fabrication of cPVC/TNT nanocomposites could potentially be used broadly in practice. Moreover, the introduction of sulfate anion radicals into the reaction system, subsequently activated by the photocatalyst under light irradiation, results in a significant enhancement in the photocatalytic efficiency [8, 30–35]. Thus, the combination of a visible-light-driven photocatalyst with the strong oxidizing capability of  $\text{SO}_4^-$  radicals can potentially lead to the highest photocatalytic performance of that specific photocatalyst under visible light.

Herein, we use the effectiveness of cPVC/TNT nanocomposites and the introduction of PMS to produce an efficient photocatalyst under visible light. Our setting also demonstrates rational stability for a set of five-repeated rounds of photocatalytic activity. We also determine to what extent  $\text{SO}_4^-$  radicals played a role in the photocatalytic enhancement in situ via trapping experiments.

## 2. Experimental

**2.1. Materials.** Commercial polyvinyl chloride (PVC), ethylene glycol (EG, 99.8%), tetrahydrofuran (THF, 99.0%), commercial  $\text{TiO}_2$  powder (Merck, 99.99%), hydrochloric acid (HCl, China, 37%), sodium hydroxide (NaOH, Merck, 99%), peroxymonosulfate (PMS), potassium iodide (KI, 99.99%), isopropyl alcohol (IPA,  $\text{C}_3\text{H}_8\text{O}$ , 99.99%), potassium dichromate ( $\text{K}_2\text{Cr}_2\text{O}_7$ , 99.99%), *tert*-butanol (TBA;  $(\text{CH}_3)_3\text{COH}$ , 99.99%), rhodamine B (RhB,  $\text{C}_{28}\text{H}_{31}\text{ClN}_2\text{O}_3$ ), and deionized (DI) water (Puris-Evo water system) were used.

### 2.2. Synthesis of Materials

**2.2.1. Synthesis of  $\text{TiO}_2$  Nanotubes (TNTs) via Hydrothermal Method.** The preparation of TNT via a hydrothermal process was reported in our previous works [36, 37]. Accordingly, 1.7 g of commercial  $\text{TiO}_2$  powder was mixed with 157 mL of 10M NaOH solution for a certain time to get a well-dispersed suspension. This mixture of  $\text{TiO}_2$  powder and NaOH solution was subsequently transferred into a Teflon

container, closely sealed by a stainless-steel autoclave. The hydrothermal process was operated at a temperature of  $135^\circ\text{C}$  for 24 h. The hydrothermally treated mixture was then naturally cooled to room temperature, followed by a pH treatment using HCl and DI water to reach a pH value of 4 and 7, respectively. TNTs were obtained by drying the product at  $60^\circ\text{C}$  for several hours.

**2.2.2. Synthesis of cPVC/TNT Nanocomposites.** The preparation of cPVC/TNT nanocomposites was reported in our recent work [29]. For preparing cPVC, first, PVC powder was added into a mixture of NaOH and ethylene glycol. Second, the three-component mixture was stirred for 30 min, followed by sonication for a further 30 min. Third, the well-dispersed mixture was transferred into a 3-neck flask, which was subsequently stirred for a certain time before treatment in nitrogen gas at  $190^\circ\text{C}$  for 3 h. Finally, cPVC was obtained by extensively washing the treated solution with DI water, followed by a drying step at  $60^\circ\text{C}$ . cPVC/TNT samples were then prepared straightforwardly. Different amounts of cPVC were dissolved in 10 mL THF. Subsequently, TNT was added into the cPVC/THF mixtures with the mass ratios (cPVC:TNT) of 10:100. The combination was then magnetically stirred for 30 min, which was sonicated for a further 30 min. Lastly, the final products were fully dried at  $60^\circ\text{C}$  for 1 h to obtain cPVC/TNT nanocomposites.

**2.3. Characterizations.** Transmission electron microscopy (TEM) images were taken on a JEM 1400 at 100 kV to observe the materials' morphology. X-ray diffraction (XRD) patterns were taken using a Bruker D8-Advance 5005 (Cu  $\text{K}\alpha$  radiation,  $\lambda = 0.154064$  nm) in the range  $2\theta$  from  $10^\circ$  to  $70^\circ$  to define the crystal structure of as-prepared materials. Also, Fourier-transform infrared spectroscopy (FTIR) spectra were captured on a JASCO-4700 to detect the vibration of molecules in the region of  $480$  to  $4000$   $\text{cm}^{-1}$ , which used KBr pellets as the reference.

**2.4. Evaluation of Photocatalytic Activity.** We used rhodamine B (RhB) as the organic pollutant in evaluating the photocatalytic degradation of our material. RhB is a water-soluble organic dye and is widely used in the textile industry. RhB can injure human eyes and skin and cause respiratory problems [38]. Furthermore, it induces phototoxicity and shows resistance to biooxidation. Thus, it is important to study the photocatalytic degradation in which RhB is the target pollutant. The photocatalytic tests were performed using 0.1 g of photocatalyst against a 60 mL rhodamine B (RhB) dye solution with a concentration of  $200$   $\text{mg L}^{-1}$ . PMS (0.1 to 5 mM) was added to the RhB dye solution before introducing the photocatalyst. The PMS-activated photocatalyst/RhB mixture was stirred in the dark for 1.5 h to achieve adsorption/desorption. Subsequently, the equilibrated system was illuminated by visible light from a simulated solar light (Osram Ultra-Vitalux 300 W) attached with a UV cutting glass. The entire photocatalytic activities were performed for 3 h. Over intervals of 30 min, a small amount of the suspension was withdrawn, followed by centrifuge at a rapid rate to separate the solution from the suspension. Shortly after, a

UV-Vis spectrophotometer (U2910, Hitachi, Japan) was used to measure the solution's absorption spectrum in the range of 400 nm to 650 nm. The photocatalytic efficiency and the photocatalytic reaction rate were quantitatively calculated via

$$\eta = \frac{C_0 - C_t}{C_0} \times 100\%, \quad (1)$$

where  $\eta$  stands for photocatalytic degradation efficiency of RhB (%),  $C_0$  regards the initial concentration of RhB, and  $C_t$  regards the concentration of RhB at time  $t$ .

**2.5. Radical Trapping Test.** The radical trapping experiments, using standard scavengers, including KI,  $K_2Cr_2O_7$ , IPA, and TBA, were performed to probe the extent of involvement in the photocatalytic reactions of the photogenerated hole, electron,  $SO_4^-$ , and  $\cdot OH$ , respectively. The concentration of the scavenger was 3 mM. The experimental conditions for these trapping experiments were like those described in the photocatalytic activity tests.

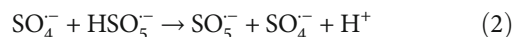
**2.6. Evaluation of Photocatalytic Stability.** After the first round of the photocatalytic activity, the photocatalyst was collected from the suspension by centrifuge at high speed and dried at 60°C. Subsequently, this collected photocatalyst was repeatedly used for further five photocatalytic activity tests to quantify the sample's stability against photocorrosion, one-time use problem, and so on.

### 3. Results and Discussion

Structural features of the as-prepared nanocomposite are characterized (Figure 1). The FTIR profile of the cPVC/TNT nanocomposite shows a prominent presence of a vibration peak at  $1628\text{ cm}^{-1}$ , representing C=C bonds in cPVC [29, 39], and the well-known vibration of the Ti-O-Ti bond at around  $500\text{ cm}^{-1}$  [40] (see Figure 1(a)). Also, this sample's XRD pattern shows the presence of anatase and rutile phase signals of  $TiO_2$  (JCPDS No. 21-1272 and No. 65-6231) and a typical diffraction peak of cPVC at  $25^\circ$  (Figure 1(b)). Thus, FTIR and XRD results have evidenced success in the fabrication of the cPVC/TNT nanocomposite. The XRD pattern also indicates a good crystallinity of the cPVC/TNT nanocomposite, which is potentially favorable for photocatalytic activity.

Changes in the morphology of TNTs upon the combination with cPVC using TEM images are presented in Figure 2. TNT has a typical hollow morphology with an outer diameter of about 9.5 nm (Figures 2(a) and 2(b)). Further morphological details of TNT, prepared via the hydrothermal method, are previously reported [41]. Upon combination with cPVC, the TNT's relatively smooth surface becomes a rough surface, which is covered with nanoscale spherical objects (Figures 2(c) and 2(d)). Those nanoscale spherical objects could be attributed to the addition of cPVC to the surface of TNT, forming a nanocomposite. Importantly, the combination of cPVC and TNT has been successfully performed without damaging TNT's unique morphology.

Photocatalytic properties of the cPVC/TNT nanocomposite against the RhB solution upon PMS activation under visible light is studied (Figure 3). It is critical to note that the photocatalytic activity of the cPVC/TNT nanocomposite has been shown to outperform that of cPVC and TNT samples completely under visible light [29]; it is thus not necessary to reconsider it in this work. A referencing test is done with no photocatalyst for 180 min of irradiation, showing no self-degradation due to the light sensitizing effect (Figure 3(a)). Also, using a RhB solution with a high concentration ( $200\text{ mg L}^{-1}$ ), we intentionally constrained the photocatalytic activity of the cPVC/TNT nanocomposite, leading to no visible light degradation of RhB. Subsequently, PMS with concentration varying from 0.1 to 5 mM is added into the photocatalytic system. Upon adding PMS, the photocatalytic performance of the cPVC/TNT nanocomposite prominently increases with a greater amount of PMS. The cPVC/TNT nanocomposite's photocatalytic activity seems to reach the highest performance upon being activated by PMS at the concentration of 3 mM, which takes only 120 min to degrade the pollutant fully. Also, the absorption spectra of RhB show a great decrease in its intensity during 120 min of reaction without shifting its typical peak, which indicates excellent photocatalytic performance (Figure 3(b)). In addition, a greater amount of PMS (4 and 5 mM) also shows good performance, but both take a longer time (150 min) to degrade RhB fully. Generally, the amount of generated  $\cdot OH$  and  $SO_4^-$  directly depends on the PMS concentration. As shown in Figure 3(a), the degradation rate of RhB is accelerated when increasing the PMS concentration from 0.1 to 3 mM. However, when the PMS concentration is increased from 3 to 5 mM, a slight reduction in RhB degradation is observed. Two reasons could interpret this result. First, an optimal PMS could serve as electron acceptors, leading to the improvement of the photocatalytic performance, whereas the photogenerated electrons might not be readily sufficient to activate the excessive PMS [30]. Second, a typical reaction could be involved in the process that happens between excessive PMS and  $SO_4^-$  radicals to give rise to the generation of  $SO_5^-$  that has a lower oxidizing ability [42], leading to the decreased performance against RhB (see equation (2)). Thus, our results show that the cPVC/TNT nanocomposite's photocatalytic performance can be enhanced significantly by PMS activation with an optimal amount of PMS at the concentration of 3 mM.



To have a better comparison with the state-of-the-art, we provide an extensive list of the current photocatalytic systems (Table 1). Key factors such as pollutant indicator, concentration of pollutants, optimal PMS concentration, amount of photocatalyst, and excitation source are tabulated. In summary, our system, cPVC/TNT/PMS/Vis, has shown competitive photocatalytic activity compared to a wide range of materials. We have used a low amount of photocatalyst in addition to a below-average PMS concentration to fully

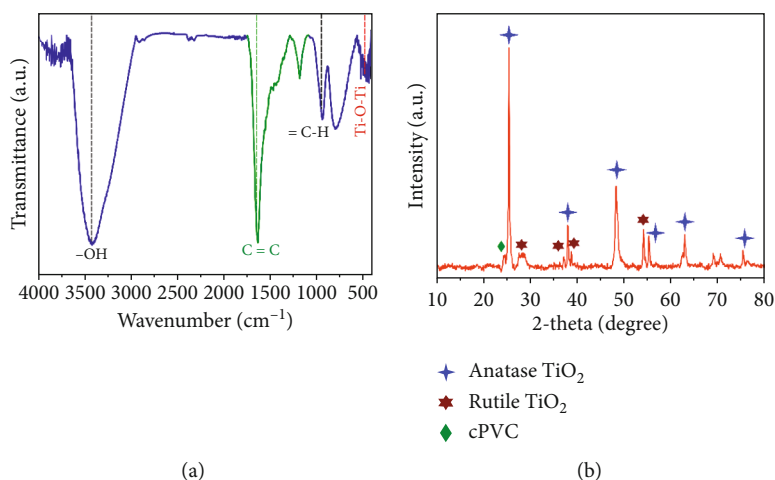


FIGURE 1: (a) FTIR spectrum and (b) XRD pattern of cPVC/TNT nanocomposite.

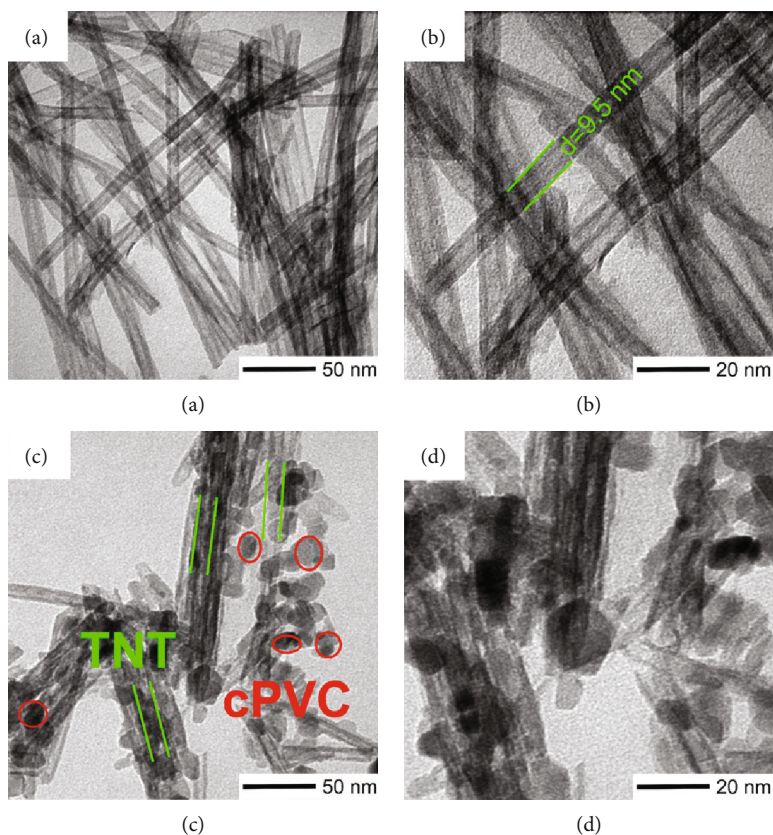


FIGURE 2: TEM image of (a, b) TNTs and (c, d) cPVC/TNT nanocomposite.

degrade RhB at a remarkably high concentration, which only uses visible light as the irradiation source.

In addition to the performance, photocatalysts having a certain benefit of recycling would allow them to be used widely in practice. By recycling the used photocatalyst, we test the photocatalytic performance of our cPVC/TNT nanocomposite against RhB with PMS's addition at the concentration of 3 mM for five repeated rounds (Figure 3(c)). Our results show that the photocatalytic performance decreases gradually after each round, which would be attributed to

the photocatalyst's loss in the postprocessing steps. However, even after five rounds of the repeated photocatalytic tests, the efficiency was still greater than 70%, which is a good merit given the remarkably high concentration of RhB as well as the use of visible light only.

Although we have shown that at a high concentration of RhB the cPVC/TNT nanocomposite's photocatalytic activity is strictly constrained, the introduction of sulfate radicals is the key factor to activate the reaction (Figure 3(a)). However, to develop a deep understanding of all radical species' extent

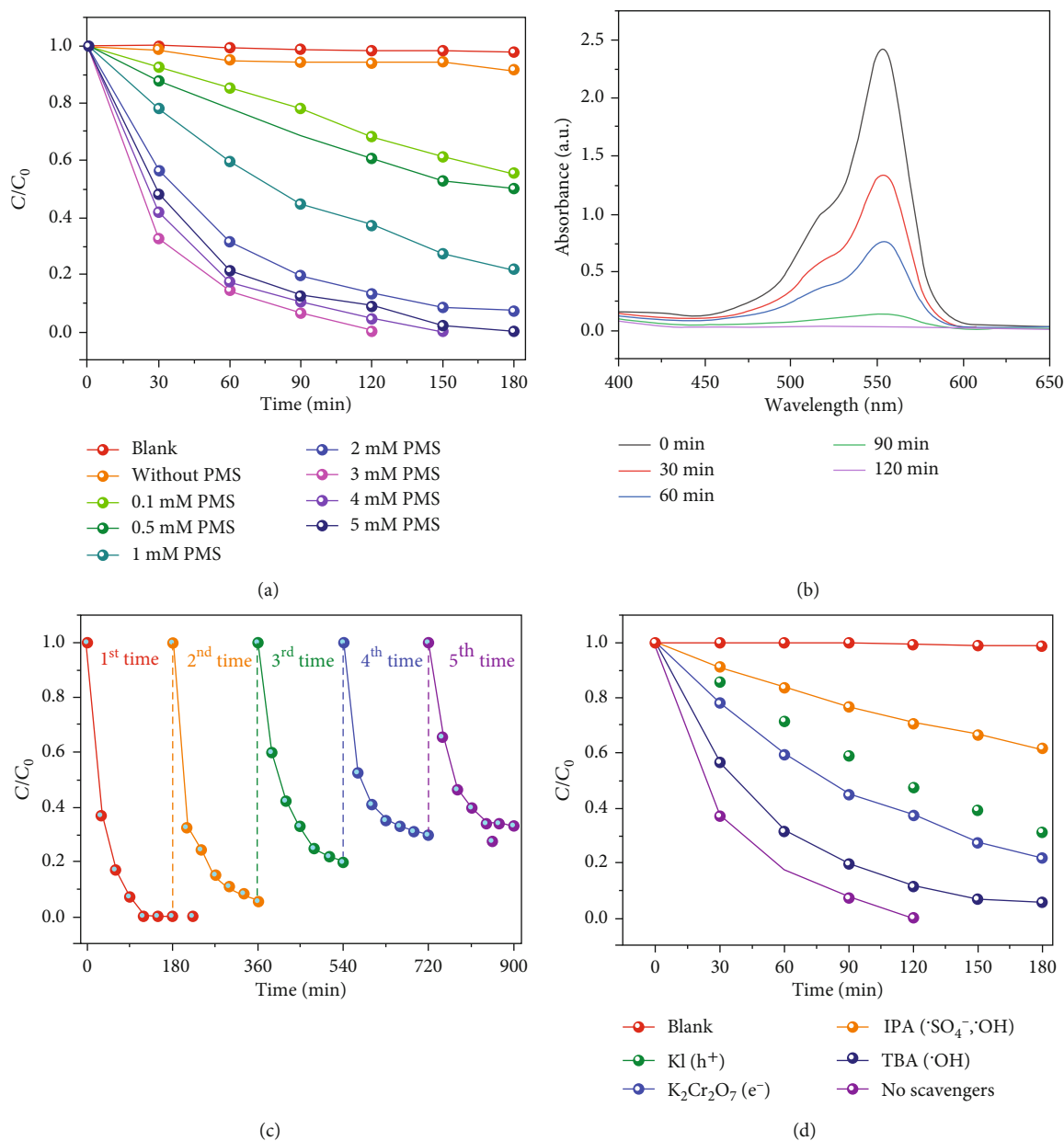


FIGURE 3: (a) Photocatalytic degradation of the cPVC/TNT nanocomposite against RhB upon PMS activation with a concentration varied from 0.1 mM to 5 mM under visible light. (b) Absorption spectra of RhB of the cPVC/TNT nanocomposite after being activated with PMS at a concentration of 3 mM during the photocatalytic reaction. (c) The photocatalytic performance of the cPVC/TNT nanocomposite after being recycled five repeated times. (d) Radical trapping test results.

of involvement during the photocatalytic reaction upon being activated by PMS, a series of trapping tests is conducted. The involvement of radical species in photocatalytic activity of the cPVC/TNT nanocomposite upon PMS activation can be classified into three groups (Figure 3(d)). The first group (using KI and  $\text{K}_2\text{Cr}_2\text{O}_7$  as scavengers) regards the partial involvement of photogenerated electrons and holes, which shows a slight decline in the photocatalytic performance. This slight reduction has resulted from the partial loss in starting reactions (both electrons and holes can activate sulfate radicals), explaining the reason for the photocatalytic activity still present despite the absence of those

electrons or holes. There is a relatively higher loss in the photocatalytic activity in trapping holes than trapping electrons, which contrasts with previous works using TNT materials [41]. This result can be explained via the supposedly higher amount of  $\text{SO}_4^-$  which can be produced from holes in comparison with electrons (see equations (4), (5), (6), (7)). The second group is with regard to the involvement of  $\cdot\text{OH}$  groups, which is usually the main factor in semiconductor-induced photocatalytic reactions. Our results show that by confining the activity of  $\cdot\text{OH}$  groups, using TBA, the photocatalytic performance on the cPVC/TNT nanocomposite upon PMS activation is affected negligibly (Figure 3(d)). This result

TABLE 1: A comparison of photocatalytic activity against RhB between current systems having been assisted by PMS activation.

Catalyst system	Pollutant conc. (mg L <sup>-1</sup> )	PMS conc. (mM)	Catalyst dosage (g L <sup>-1</sup> )	Irradiation time (min)	Efficiency (%)	Ref.
BiFeO <sub>3</sub> /PMS/Vis	5	5.0	1.0	40	60	[43]
Fe <sub>3</sub> O <sub>4</sub> /PMS/UV	383	12.0	5.0	120	80	[44]
BiVO <sub>4</sub> /PMS/Vis	10	1.0	0.5	60	97	[45]
CoFe <sub>2</sub> O <sub>4</sub> /TNT/PMS/Vis	100	4.0	0.2	60	100	[46]
Mn <sub>3</sub> O <sub>4</sub> /ZIF-8	10	0.3	0.3	60	100	[47]
α-MnO <sub>2</sub> /palygorskite/PMS/Vis	20	0.1	0.1	300	100	[48]
CuBi <sub>2</sub> O <sub>4</sub> /PMS/Vis	25	0.5	0.8	180	100	[49]
Fe-Co/PMS/UV	20	0.25	0.2	20	100	[50]
rGO/CoPc/PMS/Vis	120	0.07	0.5	40	100	[51]
cPVC/TNTs/Vis	200	3.0	0.1	120	100	This study

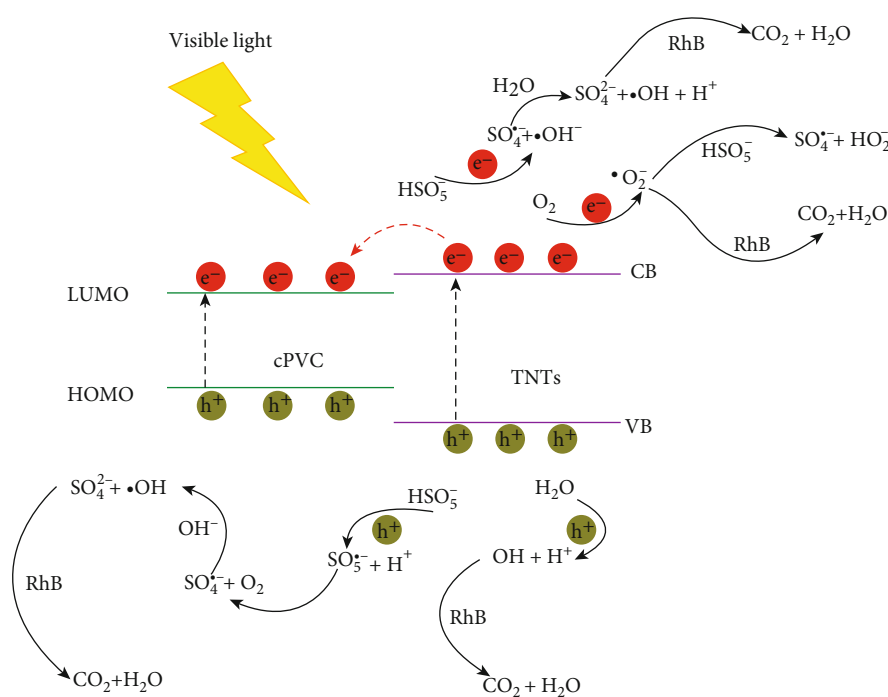


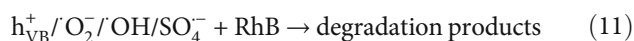
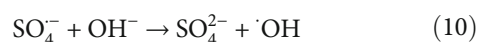
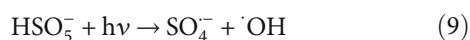
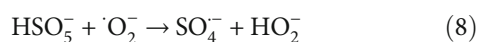
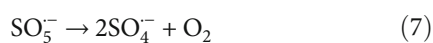
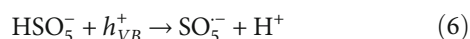
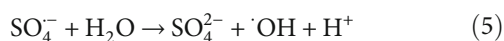
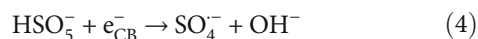
FIGURE 4: A schematic illustration of the photocatalytic degradation mechanism upon activation by PMS under visible light.

confirms the fact that in PMS-activated photocatalytic reactions, the role of  $\cdot\text{OH}$  groups is not the key in comparison to that of  $\text{SO}_4^{\bullet-}$  groups. The third group presents a case of strong confinement by trapping both  $\text{SO}_4^{\bullet-}$  and  $\cdot\text{OH}$  groups by using IPA. Our results show that the photocatalytic performance has been significantly decreased in this case.

The mechanism for the photocatalytic activity of the cPVC/TNT/PMS system under visible light is schematically illustrated in Figure 4. In the cPVC/TNT/PMS system, electrons generated from the conduction band (CB) could be used by dissolved oxygen or directly caught by the adsorbed PMS in which PMS is activated to produce  $\text{SO}_4^{\bullet-}$  (see equations (8) and (9)). Following this process is the enhanced sep-

aration of photogenerated electrons and holes. The remaining holes in the valence band (VB) could also directly oxidize pollutants due to its strong oxidation ability. Also,  $\text{SO}_4^{\bullet-}$  radicals can bring out radical interconversion reactions to yield  $\cdot\text{OH}$  by the reaction between  $\text{SO}_4^{\bullet-}$  and  $\text{OH}^-$  (see equation (10)). In our cPVC/TNT/PMS system, the photogenerated holes play a more important role than photogenerated electrons, which can be highlighted in two aspects. First, the photogenerated holes can oxidize RhB directly. Second,  $\text{SO}_5^{\bullet-}$  radicals with the lower oxidation capacity are also generated through the combination of PMS and holes (equation (6)), and the generated  $\text{SO}_5^{\bullet-}$  slightly contributed to  $\text{SO}_4^{\bullet-}/\cdot\text{OH}$  production by its self-sacrificing reactions (equation (7)).

Thus, more photogenerated carriers are effectively separated, and more electrons are transferred to participate in the photocatalytic reactions, which facilitates the PMS activation to increase further  $\text{SO}_4^-/\text{OH}$ . As a result, main active species such as holes (VB),  $\cdot\text{O}_2^-$ ,  $\cdot\text{OH}$ , and  $\text{SO}_4^-$  have contributed to the excellent catalytic activity in the developed cPVC/TNT/PMS system under visible light (see equation (11) and Figure 4), and pollutants are readily degraded into smaller intermediates and finally into  $\text{CO}_2$  and  $\text{H}_2\text{O}$ .



#### 4. Conclusions

In summary, we have prepared a visible-light-driven photocatalyst by combining conjugated polyvinyl chloride and  $\text{TiO}_2$  nanotubes via a simple thermolysis method. The introduction of PMS at the concentration of 3 mM has significantly enhanced the photocatalytic performance of the nanocomposite, which is also photostable and recycled with good performance. By confining the active radicals, we have determined that  $\text{SO}_4^-$  radicals are the key factor for enhancing the photocatalytic performance. Also, photogenerated holes are greater than photogenerated electrons in the extent of involvement. Production of a high-performance photocatalyst under visible light via a simple, inexpensive process will lead to wide use in practice.

#### Data Availability

The data used to support the findings of this study are available from the corresponding author upon request.

#### Conflicts of Interest

The authors declare that they have no conflicts of interest.

#### Authors' Contributions

La Phan Phuong Ha and Tran Hong Huy contributed equally to this work.

#### Acknowledgments

The authors would like to acknowledge the support from the Vietnam National University Ho Chi Minh City and the CM

Thi Laboratory. This work is funded by Vietnam National University Ho Chi Minh City (VNU-HCM) under grant number 562-2020-18-05.

#### References

- [1] M. A. Fox and M. T. Dulay, "Heterogeneous photocatalysis," *Chemical Reviews*, vol. 93, no. 1, pp. 341–357, 1993.
- [2] M. R. Hoffmann, S. T. Martin, W. Choi, and D. W. Bahnemann, "Environmental applications of semiconductor photocatalysis," *Chemical Reviews*, vol. 95, no. 1, pp. 69–96, 1995.
- [3] C. Xu, P. R. Anusuyadevi, C. Aymonier, R. Luque, and S. Marre, "Nanostructured materials for photocatalysis," *Chemical Society Review*, vol. 48, no. 14, pp. 3868–3902, 2019.
- [4] T. H. Huy, B. D. Phat, C. M. Thi, and P. Van Viet, "High photocatalytic removal of NO gas over  $\text{SnO}_2$  nanoparticles under solar light," *Environmental Chemistry Letters*, vol. 17, no. 1, pp. 527–531, 2019.
- [5] T. P. Yoon, M. A. Ischay, and J. Du, "Visible light photocatalysis as a greener approach to photochemical synthesis," *Nature Chemistry*, vol. 2, no. 7, pp. 527–532, 2010.
- [6] R. Asahi, T. Morikawa, T. Ohwaki, K. Aoki, and Y. Taga, "Visible-light photocatalysis in nitrogen-doped titanium oxides," *Science*, vol. 293, no. 5528, pp. 269–271, 2001.
- [7] M. Ahmad, A. L. Teel, and R. J. Watts, "Mechanism of persulfate activation by phenols," *Environmental Science & Technology*, vol. 47, no. 11, pp. 5864–5871, 2013.
- [8] Y. Y. Ahn, E. T. Yun, J. W. Seo et al., "Activation of peroxymonosulfate by surface-loaded noble metal nanoparticles for oxidative degradation of organic compounds," *Environmental Science & Technology*, vol. 50, no. 18, pp. 10187–10197, 2016.
- [9] G. P. Anipsitakis and D. D. Dionysiou, "Degradation of organic contaminants in water with sulfate radicals generated by the conjunction of peroxymonosulfate with cobalt," *Environmental Science & Technology*, vol. 37, no. 20, pp. 4790–4797, 2003.
- [10] Y. Chen, G. Zhang, H. Liu, and J. Qu, "Confining free radicals in close vicinity to contaminants enables ultrafast Fenton-like processes in the interspacing of  $\text{MoS}_2$  membranes," *Angewandte Chemie International Edition*, vol. 58, no. 24, pp. 8134–8138, 2019.
- [11] J. Du, J. Bao, Y. Liu, S. H. Kim, and D. D. Dionysiou, "Facile preparation of porous  $\text{Mn}/\text{Fe}_3\text{O}_4$  cubes as peroxymonosulfate activating catalyst for effective bisphenol A degradation," *Chemical Engineering Journal*, vol. 376, article 119193, 2019.
- [12] X. Duan, Z. Ao, H. Zhang et al., "Nanodiamonds in  $\text{sp}^2/\text{sp}^3$  configuration for radical to nonradical oxidation: core-shell layer dependence," *Applied Catalysis B: Environmental*, vol. 222, pp. 176–181, 2018.
- [13] X. Cheng, H. Guo, Y. Zhang, G. V. Korshin, and B. Yang, "Insights into the mechanism of nonradical reactions of persulfate activated by carbon nanotubes: activation performance and structure-function relationship," *Water Research*, vol. 157, pp. 406–414, 2019.
- [14] X. Duan, H. Sun, Y. Wang, J. Kang, and S. Wang, "N-Doping-induced nonradical reaction on single-walled carbon nanotubes for catalytic phenol oxidation," *ACS Catalysis*, vol. 5, no. 2, pp. 553–559, 2015.
- [15] X. Lu, J. Zhao, Q. Wang et al., "Sonolytic degradation of bisphenol S: effect of dissolved oxygen and peroxydisulfate,

- oxidation products and acute toxicity," *Water Research*, vol. 165, article 114969, 2019.
- [16] Y. Qin, G. Li, Y. Gao, L. Zhang, Y. S. Ok, and T. An, "Persistent free radicals in carbon-based materials on transformation of refractory organic contaminants (ROCs) in water: a critical review," *Water Research*, vol. 137, pp. 130–143, 2018.
- [17] B. Xu, T. Ding, Y. Zhang, Y. Wen, Z. Yang, and M. Zhang, "A new efficient visible-light-driven composite photocatalyst comprising ZnFe<sub>2</sub>O<sub>4</sub> nanoparticles and conjugated polymer from the dehydrochlorination of polyvinyl chloride," *Materials Letters*, vol. 187, pp. 123–125, 2017.
- [18] Y. Zhang, F. Zhang, Z. Yang, H. Xue, and D. D. Dionysiou, "Development of a new efficient visible-light-driven photocatalyst from SnS<sub>2</sub> and polyvinyl chloride," *Journal of Catalysis*, vol. 344, pp. 692–700, 2016.
- [19] S. Debnath, N. Ballav, H. Nyoni, A. Maity, and K. Pillay, "Optimization and mechanism elucidation of the catalytic photodegradation of the dyes Eosin Yellow (EY) and Naphthol blue black (NBB) by a polyaniline-coated titanium dioxide nanocomposite," *Applied Catalysis B: Environmental*, vol. 163, pp. 330–342, 2015.
- [20] L. Liu, L. Ding, Y. Liu et al., "A stable Ag<sub>3</sub>PO<sub>4</sub>@PANI core@shell hybrid: enrichment photocatalytic degradation with  $\pi$ - $\pi$  conjugation," *Applied Catalysis B: Environmental*, vol. 201, pp. 92–104, 2017.
- [21] J. Zhang, H. Yang, S. Xu et al., "Dramatic enhancement of visible light photocatalysis due to strong interaction between TiO<sub>2</sub> and end-group functionalized P3HT," *Applied Catalysis B: Environmental*, vol. 174–175, pp. 193–202, 2015.
- [22] P. D. Bui, H. H. Tran, F. Kang et al., "Insight into the photocatalytic mechanism of tin dioxide/polyaniline nanocomposites for no degradation under solar light," *ACS Applied Nano Materials*, vol. 1, no. 10, pp. 5786–5794, 2018.
- [23] Y. Bai, K. Nakagawa, A. J. Cowan et al., "Photocatalyst Z-scheme system composed of a linear conjugated polymer and BiVO<sub>4</sub> for overall water splitting under visible light," *Journal of Materials Chemistry A*, vol. 8, no. 32, pp. 16283–16290, 2020.
- [24] V. V. Pham, D. P. Bui, H. H. Tran et al., "Photoreduction route for Cu<sub>2</sub>O/TiO<sub>2</sub> nanotubes junction for enhanced photocatalytic activity," *RSC Advances*, vol. 8, no. 22, pp. 12420–12427, 2018.
- [25] T. K. Truong, T. Van Doan, H. H. Tran et al., "Effect of Cr doping on visible-light-driven photocatalytic activity of ZnO nanoparticles," *Journal of Electronic Materials*, vol. 48, no. 11, pp. 7378–7388, 2019.
- [26] P. Van Viet, T. H. Huy, T. T. Sang, H. M. Nguyet, and C. M. Thi, "One-pot hydrothermal synthesis of Si doped TiO<sub>2</sub> nanotubes from commercial material sources for visible light-driven photocatalytic activity," *Materials Research Express*, vol. 6, no. 5, article 055006, 2019.
- [27] E. Fenelon, D.-P. Bui, H. H. Tran et al., "Straightforward synthesis of SnO<sub>2</sub>/Bi<sub>2</sub>S<sub>3</sub>/BiOCl–Bi<sub>24</sub>O<sub>31</sub>Cl<sub>10</sub> Composites for drastically enhancing rhodamine B photocatalytic degradation under visible light," *ACS Omega*, vol. 5, no. 32, pp. 20438–20449, 2020.
- [28] D. P. Bui, M. T. Nguyen, H. H. Tran, S. J. You, Y. F. Wang, and P. van Viet, "Green synthesis of Ag@SnO<sub>2</sub> nanocomposites for enhancing photocatalysis of nitrogen monoxide removal under solar light irradiation," *Catalysis Communications*, vol. 136, article 105902, 2020.
- [29] D.-P. Bui, H. Pham, T. Cao, and V. Pham, "Preparation of conjugated polyvinyl chloride/TiO<sub>2</sub> nanotubes for rhodamine B photocatalytic degradation under visible light," *Journal of Chemical Technology & Biotechnology*, vol. 95, pp. 2707–2714, 2020.
- [30] F. Chen, G. X. Huang, F. B. Yao et al., "Catalytic degradation of ciprofloxacin by a visible-light-assisted peroxymonosulfate activation system: performance and mechanism," *Water Research*, vol. 173, article 115559, 2020.
- [31] Y. Wang, X. Zhao, D. Cao, Y. Wang, and Y. Zhu, "Peroxymonosulfate enhanced visible light photocatalytic degradation bisphenol A by single-atom dispersed Ag mesoporous g-C<sub>3</sub>N<sub>4</sub> hybrid," *Applied Catalysis B: Environmental*, vol. 211, pp. 79–88, 2017.
- [32] J. Lim, D. Y. Kwak, F. Sieland, C. Kim, D. W. Bahnemann, and W. Choi, "Visible light-induced catalytic activation of peroxymonosulfate using heterogeneous surface complexes of amino acids on TiO<sub>2</sub>," *Applied Catalysis B: Environmental*, vol. 225, pp. 406–414, 2018.
- [33] Y.-Y. Ahn, H. Bae, H. I. Kim et al., "Surface-loaded metal nanoparticles for peroxymonosulfate activation: efficiency and mechanism reconnaissance," *Applied Catalysis B: Environmental*, vol. 241, pp. 561–569, 2019.
- [34] J. Lee, U. von Gunten, and J. H. Kim, "Persulfate-based advanced oxidation: critical assessment of opportunities and roadblocks," *Environmental Science Technology*, vol. 54, no. 6, pp. 3064–3081, 2020.
- [35] B. C. Hodges, E. L. Cates, and J. H. Kim, "Challenges and prospects of advanced oxidation water treatment processes using catalytic nanomaterials," *Nature Nanotechnology*, vol. 13, no. 8, pp. 642–650, 2018.
- [36] P. Van Viet, T. H. Huy, S.-J. You, L. Van Hieu, and C. M. Thi, "Hydrothermal synthesis, characterization, and photocatalytic activity of silicon doped TiO<sub>2</sub> nanotubes," *Superlattices and Microstructures*, vol. 123, pp. 447–455, 2018.
- [37] P. Van Viet, T. H. Huy, N. X. Sang, C. M. Thi, and L. Van Hieu, "One-step hydrothermal synthesis and characterisation of SnO<sub>2</sub> nanoparticle-loaded TiO<sub>2</sub> nanotubes with high photocatalytic performance under sunlight," *Journal of Materials Science*, vol. 53, no. 5, pp. 3364–3374, 2018.
- [38] J. Sarma, A. Sarma, and K. G. Bhattacharyya, "Biosorption of commercial dyes on *Azadirachta indica* leaf powder: a case study with a basic dye rhodamine B," *Industrial & Engineering Chemistry Research*, vol. 47, no. 15, pp. 5433–5440, 2008.
- [39] S. Narita, S. Ichinohe, and S. Enomoto, "Infrared spectrum of polyvinyl chloride. I," *Journal of Polymer Science*, vol. 37, no. 131, pp. 273–280, 1959.
- [40] V. A. Zeitler and C. A. Brown, "The infrared spectra of some Ti-O-Si, Ti-O-Ti and Si-O-Si compounds," *The Journal of Physical Chemistry*, vol. 61, no. 9, pp. 1174–1177, 1957.
- [41] T. H. Huy, D. P. Bui, F. Kang et al., "SnO<sub>2</sub>/TiO<sub>2</sub> nanotube heterojunction: the first investigation of NO degradation by visible light-driven photocatalysis," *Chemosphere*, vol. 215, pp. 323–332, 2019.
- [42] C. Cai, J. Liu, Z. Zhang, Y. Zheng, and H. Zhang, "Visible light enhanced heterogeneous photo-degradation of orange II by zinc ferrite (ZnFe<sub>2</sub>O<sub>4</sub>) catalyst with the assistance of persulfate," *Separation and Purification Technology*, vol. 165, pp. 42–52, 2016.
- [43] F. Chi, B. Song, B. Yang, Y. Lv, S. Ran, and Q. Huo, "Activation of peroxymonosulfate by BiFeO<sub>3</sub> microspheres under visible



- light irradiation for decomposition of organic pollutants,” *RSC Advances*, vol. 5, no. 83, pp. 67412–67417, 2015.
- [44] Y. Leng, W. Guo, X. Shi et al., “Degradation of rhodamine B by persulfate activated with  $\text{Fe}_3\text{O}_4$ : effect of polyhydroquinone serving as an electron shuttle,” *Chemical Engineering Journal*, vol. 240, pp. 338–343, 2014.
- [45] Y. Liu, H. Guo, Y. Zhang, W. Tang, X. Cheng, and H. Liu, “Activation of peroxymonosulfate by  $\text{BiVO}_4$  under visible light for degradation of rhodamine B,” *Chemical Physics Letters*, vol. 653, pp. 101–107, 2016.
- [46] Y. Du, W. Ma, P. Liu, B. Zou, and J. Ma, “Magnetic  $\text{CoFe}_2\text{O}_4$  nanoparticles supported on titanate nanotubes ( $\text{CoFe}_2\text{O}_4/\text{TNTs}$ ) as a novel heterogeneous catalyst for peroxymonosulfate activation and degradation of organic pollutants,” *Journal of Hazardous Materials*, vol. 308, pp. 58–66, 2016.
- [47] L. Hu, G. Deng, W. Lu, Y. Lu, and Y. Zhang, “Peroxymonosulfate activation by  $\text{Mn}_3\text{O}_4$ /metal-organic framework for degradation of refractory aqueous organic pollutant rhodamine B,” *Chinese Journal of Catalysis*, vol. 38, no. 8, pp. 1360–1372, 2017.
- [48] C. Huang, Y. Wang, M. Gong, W. Wang, Y. Mu, and Z.-H. Hu, “ $\alpha\text{-MnO}_2$ /palygorskite composite as an effective catalyst for heterogeneous activation of peroxymonosulfate (PMS) for the degradation of rhodamine B,” *Separation and Purification Technology*, vol. 230, article 115877, 2020.
- [49] Y. Wang, F. Li, T. Xue et al., “Heterogeneous activation of peroxymonosulfate by hierarchical  $\text{CuBi}_2\text{O}_4$  to generate reactive oxygen species for refractory organic compounds degradation: morphology and surface chemistry derived reaction and its mechanism,” *Environmental Science and Pollution Research*, vol. 25, no. 5, pp. 4419–4434, 2018.
- [50] C. Gong, F. Chen, Q. Yang et al., “Heterogeneous activation of peroxymonosulfate by Fe-Co layered double hydroxide for efficient catalytic degradation of rhodamine B,” *Chemical Engineering Journal*, vol. 321, pp. 222–232, 2017.
- [51] C. Marinescu, M. Ben Ali, A. Hamdi et al., “Cobalt phthalocyanine-supported reduced graphene oxide: a highly efficient catalyst for heterogeneous activation of peroxymonosulfate for rhodamine B and pentachlorophenol degradation,” *Chemical Engineering Journal*, vol. 336, pp. 465–475, 2018.